

Measurement of the defects (cracks) of clay mixing sodium chloride 'NaCl' with consideration of the temperature Variations

Thy TRUC DOAN^{1,4*}, Hien HO THU^{1,3}, Thang NGUYEN DANH^{2,3}

¹ University of Science, Ho Chi Minh City, Vietnam, 227 Nguyen Van Cu, Cho Quan Ward, Ho Chi Minh City, Vietnam

² University of Technology, Ho Chi Minh City, Vietnam, 268 Ly Thuong Kiet, Dien Hong Ward, Ho Chi Minh City, Vietnam

³ Vietnam National University, Ho Chi Minh City, Vietnam, Dong Hoa Ward, Ho Chi Minh City, Vietnam

⁴ Kien Giang University, Vietnam, 320A- 61 Highway, Vinh Hoa Hiep, Chau Thanh District, An Giang Province, Vietnam.

* Corresponding email: dtthy@vnkgu.edu.vn

Abstract: *Measurement of the defects (cracks) of clay mixing sodium chloride 'NaCl' with consideration of the temperature variations were measured carefully by the experiment method in the laboratory. Sodium Chloride 'NaCl' concentration varied in range 9.86 - 60.56% according to the temperature range 20 - 200⁰C. The research results present clear defects (cracks) that appear much more on the body sample with a large length, width, and depth according to the different temperature variations. Moreover, the Image J software was used to analyze, calculate, and draw the defect's shape. In addition, the Unconfined Compression Test (UCT) described the close relationship between the stress and strain, the displacement and loads of the clay mixing sodium chloride 'NaCl' concentration, loading, and temperature. The maximum load is compared with the lower loading and the lower clay's resistance. Finally, these research results are good documents that contributed to the development of design, survey, and construction in geology and civil engineering to research clay near the coastal areas where clay soils are often affected by saltwater intrusion.*

Keywords: *Defect (crack); Clay Mixing Sodium Chloride 'NaCl'; Temperature variations; Stress and strain curve; Displacement and load curve*

1. Introduction

In recent decades, crack research has been done with clay soil and other soil, particularly by many methods around the world. However, the research is based on interferometry data from the Ivughli salt dome in the West Azerbaijan province of Iran. The results show that the faults are related to the cracks located around the Ivughli salt dome, and this displacement of the folded layers has caused the settlement of a part of the dome (Alizadeh Akram and Dargahi Khatoon, 2024). The behavior of the electrochemical erosion of Al_{0.5}CoCrFeNi_{0.4} (HEA) in a high-entropy alloy (HES) in 3.5% NaCl solution was measured. Results demonstrated that the Al_{0.5}CoCrFeNi_{0.4} (HEA) is high and results of the surface layer will be created on the surface HEA (Bo-wei et al., 2024). On the other hand, the research was conducting on the combination of ferromagnetic components with the support of NaCl-containing cobalt salts. Results of nanocomposite Co/C materials made in the bandwidth with 6 GHz absorption and minimal reflection loss over 60 dB (Chuanxin et al., 2023). In addition, a combination of an electric 'ERI', the system of the 'ABEM Tetramer LS', and the 2-D Inversion Modeling Software were used to determine the stress cracks. Results show that the cracks' depths decreased by up to 30% compared with the actual depths under the street surface (Colpo et al., 2022). Moreover, the linear dimension finite element method "LDFEM" was used for the simulation of the clay soil bar curve. The clay soil bar includes 7 grams of clay soil, 7 grams of cement, and 2 grams of sand. This mixture is shown in the ratio of 7:7:2. The results show that the crack width 'B' and the crack depth 'W' are big values (Neyamadpour, 2018). The nonlinear finite element method (NFEM) was used to calculate the soil cracks' influence on displacement and deformation. The results show that the crack values are big, and the lengths, widths, and depths appeared remarkably in the unsaturated soil (Namdar, 2022). Moreover, an experimental model 'Lysmeter' was used to measure the soil cracks by the experimental method. Results presented that the crack's deeps are too dry and the big flows after the soil surface is tight (Greve et al., 2010). Additionally, the research used a tension 'infiltrimeter' tool to measure the crack of the saturated soil. Results show that a high hydraulic

conductivity demonstrates a high permeable ability so the big cracks appeared much more between the soil structures (Ulén et al., 2014). From the above analysis, it is essential to show the defects (cracks) of the clay soil with the temperature variations. This research sets up a measurement of the soil clay's cracks on the sample bodies with the temperature changes from 20⁰, 40, 60, 105, 120, 150, 180, 200⁰C, and sodium chloride (NaCl) components. The relationship between the max loading and displacement is determined carefully and in combination with the stress and strain curve values with NaCl's different components. The 'Image J' software was used to analyze and draw the crack's shapes. When the increased temperature and loading make in the clear displacement, strains, stress, and cracks appear much more on the sample bodies.

From the above analysis, it is essential to consider and conclude that the cracks measurement of the clay soil with the temperature and sodium chloride "NaCl" changing that combined with behavior of deformation (or strain, displacement) with loading and stress variations is essential to be done urgently. Especially, the clay soil is located underground where high seawater levels and frequent sea level intrusion, so this clay soil needs to be researched carefully to give reliable research results for references in geology and civil engineering design and construction in the future.

3. Methodology

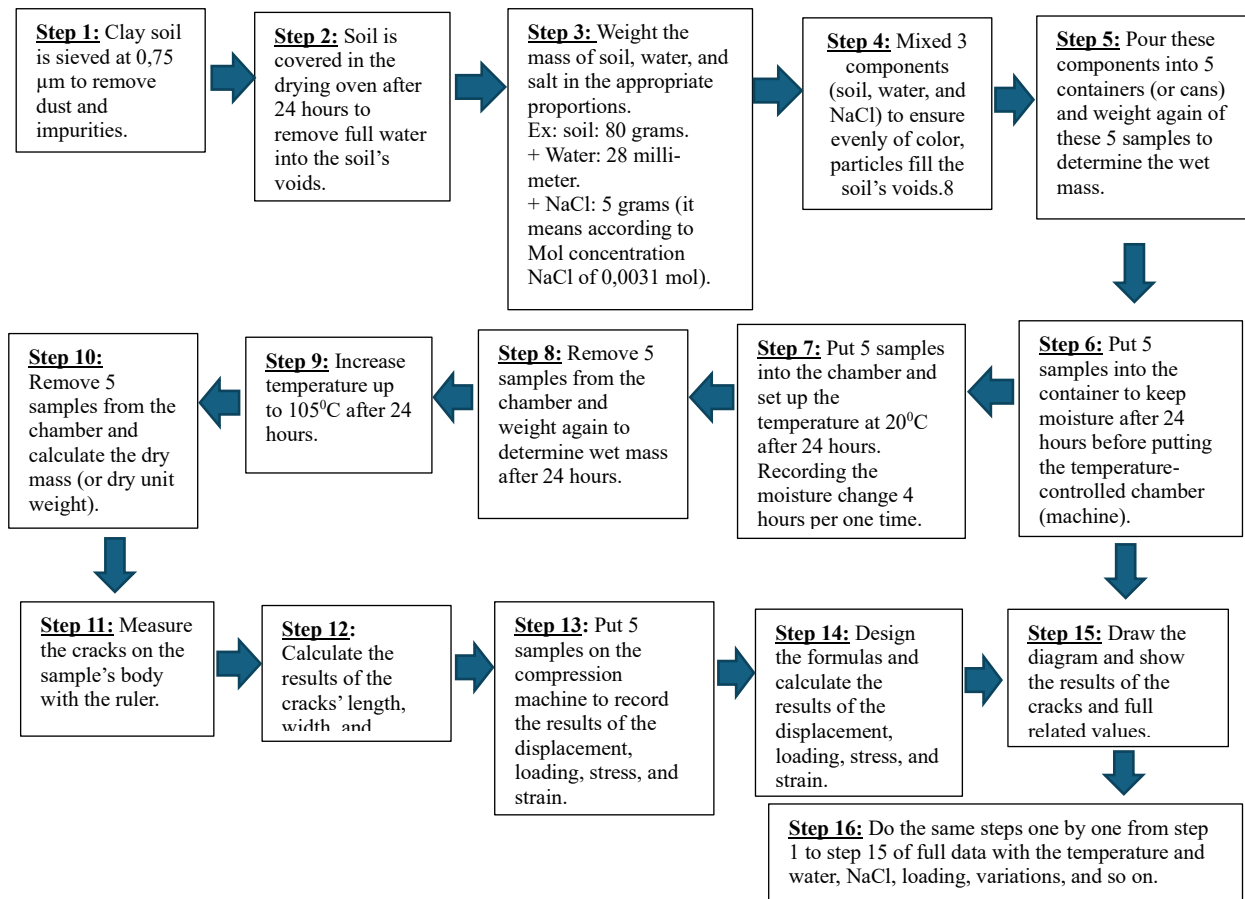
3.1 Materials

The sample's size shows 50mm of diameter and 30mm of height. The outer and initial area of the soil sample before the clay sample is placed in the oven and dried at the appropriate temperature. And this soil sample's area is calculated as: $\pi D^2/4 = 3.14 \times 50 \times 50 = 1962.5 \text{ mm}^2$. A sieve of 0.75 micrometer diameter is used for sieving clay. The liquid limit has an approximate value of WL = 55% compared with the plastic limit of WP = 50%. Clay soil samples are kept moist after 24 hours. Moisture values are set up in the range 35 - 80%. The clay soil is used at a quantity of 80 grams for each test. Temperature variations are set up from 20⁰C to 200⁰C which includes 20⁰C, 60, 90, 105, 120, 150, 180, and 200⁰C by the machines' support 'Odometer - temperature machine'. The percentage of sodium chloride (% NaCl) variations changed from 9.86 - 63.64% (Figure 1). 40 samples were collected and signed carefully to avoid confusion between samples. The 'Image J' software was used to draw and analyze the shapes of cracks on the bodies' samples. This software is supported by the "Laptop 3 Mien" company copyright in Vietnam and version 2024 (<https://laptop3mien.vn/tai-imagej-2024-link-google-da-test-100-va-huong-dan-cai-dat-full/>).

The cracks's lengths, widths, and depths are determined by the ruler in the laboratory. The loading values are set up from 0 N/mm² to 8000 N/mm² to measure the displacement, strain, and stress by the machines' support 'HEICO-UNCT' machine (Figure 1). The implementation process includes 16 steps which are done in the diagram below.

3.1.2 Calibration of machine parameters calculated values

As an example of calibration of machine parameters the sample "S1" with concentration "Mol" of solution "NaCl" $M_{\text{NaCl}} = 0.00153 \text{ mol}$ is presented. The percentage of solution "NaCl", P% = 47.17%. Temperature is 105⁰C. The result of the maximum strain of 0,1277 mm according to the stress is 0,5349 (N/m²). The full implement processes are done from the step 1 to the step 16 (diagram below). The calibration of machine parameters calculated values are shown in Table 1.



Tab. 1. Calibration of machine parameters calculated values

Points of displacements	Actual Reading from the machine		Calibration values		Strains and Stress				
	Displacement	Loading	Displacement	Loading	*Load (N)	Sample's height (mm)	Strain (mm)	Area of sample (mm ²)	Stress (N/mm ²)
A	B	C	D	E	F	G	H	K	L
1	6,9200	91,0000	0,0000	0,0000	0,0000	30	0,0000	1962,5000	0,0000
2	7,0800	93,0000	0,1600	2,0000	19,6200	30	0,0053	1.962,50000	0,0000
3	7,2500	95,0000	0,3300	4,0000	39,2400	30	0,0110	1.962,50000	0,0100
4	7,4500	96,0000	0,5300	5,0000	49,0500	30	0,0177	1.962,50000	0,0200
5	7,5900	98,0000	0,6700	7,0000	68,6700	30	0,0223	1.962,50000	0,0350
....
20	10,75	198,0000	3,8300	107,000	1049,67	30	0,1277	1.962,50000	0,5349
....
24	12,1000	169,0000	5,1800	78,0000	765,1800	30	0,1272	1.962,50000	0,3899

***Note:**

The column **D** value is according to the column **A** and line **1** location: The number zero "0" is the Displacement's Calibration at the initial location $A1 = "6,92 - 6,92"$.

The column **E** value is according to the column **A** and line **1** location: The number zero "0" at the Loading's Calibration at the initial location = $"91,00*9,81"$.

The column **H** value is according to column **A** and line **1** location: The number zero "0" at the **Strain** at the initial location = $"Displacement's Calibration/ Sample's height"$.

The column **K** value is according to column **A** and line **1** Location: Area of sample: $"1962,5" = "3,14*50*50"$. The sample's height: $H = 30$ mm. Diameter: $d = 50$ mm. The sample's material is made of copper.

The loading is converted from "kgf" into "Niuton" = $"load*9.81"$; $1 \text{ kPa} = 0.01\text{kg/cm}^2$.

The column **L** of column **A** and line **1** location: The number zero “0” at the “**Stress**” at the initial location = “Loading's Calibration/Are of sample”.

Column **A** at line 20 is the maximum value of strains and stress.



a) Samples are kept moist after 24 hours



b) Samples are signed to prepare for doing the unconfined compression test



c) Temperature - controlled chamber d) Box controls temperature chamber

Fig. 1. Samples, machine preparations to do experiments

3.2 Theoretical basis

The samples are signed carefully to minimize errors and confusion between them. A total of 40 samples were measured with the different water content and %NaCl. The theoretical basis included formulas and calculations in this research were also used in the literature issue (Thy, 2024a). *Example: The sample is signed ‘S100311515’ that is explained below:

+ ‘S1’ is centration "Mol" of solution "NaCl" $M_{NaCl} = 0.0031$ mol.

+ Number ‘1515’ is the percentage of concentration of solution "NaCl", $P\% = 15.15\%$.

3.2.1 Water contents W (1) (Thy, 2024):

$$W\% = \left[\frac{M_{wet} - M_{dry}}{M_{dry} - M_{cup}} \right] \times 100\% \quad (1)$$

Whereas, M_{wet} = Mass of the sample at the initial state, gram(g)

M_{dry} = Mass of the sample after 24 hours at 105°C, gram(g)

M_{cup} = Mass of cups which contains soil, gram(g)

3.2.2 Maximum depth of the cracks (Thy, 2024):

+ Total of solute Mol mass of Sodium Chloride” NaCl”:

$$M_{NaCl} = M_{Na} + M_{Cl} \quad (2)$$

+ The number of Mol solute Sodium Chloride “NaCl”:

$$M_{NM} = M_{salt} / M_{NaCl} \quad (3)$$

+ The number of solutes in water or Concentration "Mol" of Sodium Chloride solution in water:

$$x = M_{NM} / M_{water} \quad (4)$$

+ The Maximum depth of Cracks:

$$D_{maxcr} = f(x) = e^x \quad (5)$$

Whereas, M_{Na} is the specific Mass (Mol mass) of Sodium solute “Na”; gram/mol (g/mol);

MCl is the specific Mass (Mol mass) of Chloride solute “Cl”; gram/mol (g/mol); M_{NaCl} is the total solute Mol mass of Sodium Chloride” NaCl”; gram/mol (g/mol); M_{NM} is the number of Mol solute Sodium Chloride “NaCl; mol; M_{salt} is the mass of Sodium Chloride used actually; grams (g); x is the Concentration Mol of the solution “NaCl”; mol; D_{maxcr} is the maximum depth of cracks; millimeters (mm); e is the natural Exponential or the natural Logarithm, this value is rounded to an integer; and dimensionless; $f(x)$ is the primitive of a function; millimeters (mm).

3.2.3 Maximum length of the cracks (Thy, 2024)

The maximum length of the cracks was calculated for the total solute Mol mass of Sodium Chloride” NaCl” (see formula 2 in the section of the maximum crack depths).

+ The number of Mol solute Sodium Chloride “NaCl” was calculated with the formula:

$$\Psi = M_{salt} / M_{NaCl} \tag{6}$$

+ The number of solutes in water or Concentration "Mol" of Sodium Chloride solution in water:

$$\Delta = \Psi * x \tag{7}$$

+ The maximum length of Cracks:

$$L_{maxcr} = C + e^{\Delta} = f(\Delta) = e^{\Delta} \tag{8}$$

Whereas, Ψ is the number of Mol solute Sodium Chloride “NaCl”; mol. M_{salt} is the mass of Sodium Chloride used actually; gram (g); Δ is the number of solutes in water or Concentration "Mol" of Sodium Chloride solution in water; mol; C is the experiment value, “constant”; $C = 155$; millimeter (mm); $f(\Delta)$ is the primitive of a function; dimensionless; e is the natural exponential or the natural logarithm, this value is rounded to an integer; dimensionless; L_{maxcr} is the maximum length of cracks; millimeter (mm).

4. Results

4.1 Results of the defects (cracks) on the sample’s bodies at the temperature and NaCl concentration variations.

The sample S28.21 at 60°C and 105°C temperature after 24 hours with the sodium chloride concentration ‘NaCl’ shows many cracks that developed the width and extended the length near the body's bottom, compared with smaller cracks that appear in the middle of the sample bodies. However, the closer to the top of the sample surface, the less cracks appear. It is easier to see clearly that S36.23 at 105°C temperature, the increase of the sodium chloride ‘NaCl’ is 36.23% resulting in the cracks appearing less. Moreover, on the sample’s surface, the sodium chloride concentration ‘NaCl’ shows uneven expression. The salt crystals precipitated into white crystalline masses and formed pure white patches. Otherwise, in sample S23.40 at 90°C and a salt content of 23.40%, the phenomenon of salt crystals forming on the surface no longer appeared much, but these salt crystals mixed with soil particles appeared more around the sample body. Furthermore, as the temperature increased (150°C) along with the salt content of sample S50.68, the cracks appeared more and more larger. On the contrary, sample S54.43 clearly showed fewer cracks when the temperature increased to 180°C corresponding to the salt content of 54.43%. Moreover, sample S10.20 at 200°C presents an interaction between salt molecules and soil particles the salt crystals dissolve evenly and blend, hiding deep into the clay molecules when the water content increases and the salt content also increases. The cracks are almost small and do not appear on the entire surface of the sample body, which also proves that when the salt content is high, the ability to prevent cracks is high, the salt crystals have filled many pores in the soil, creating a tight bond between soil molecules, hindering the movement between particles in the pores. Therefore, the soil with a tighter bond between the salt crystals and soil particles occurred during full creation process.

4.2 Results of the crack's length, width, and depths at the temperature and NaCl concentration variations.

The crack length varies from 52.00mm; to 63.00mm; 180.00mm; and 40.00mm corresponding to the temperature changes at 20°C; 60°C; 120°C; and 200°C. In contrast, the crack length equals 156.30mm at 90°C; 105°C; 150°C; and 180°C. In addition, the crack width reaches its maximum at different temperature: from 20°C to 200°C. Compared with the crack length and width, the depth has a relatively small variation of 12mm at the temperature of 20°C and 60°C; and reaches 10mm at the temperature of 1800C and 2000C; reaching the value of 30mm; 50mm; 18mm; and 15mm corresponds to temperatures 90°C; 105°C; 120°C; and 150°C. The crack shapes on the sample body are shown in Fig 2.

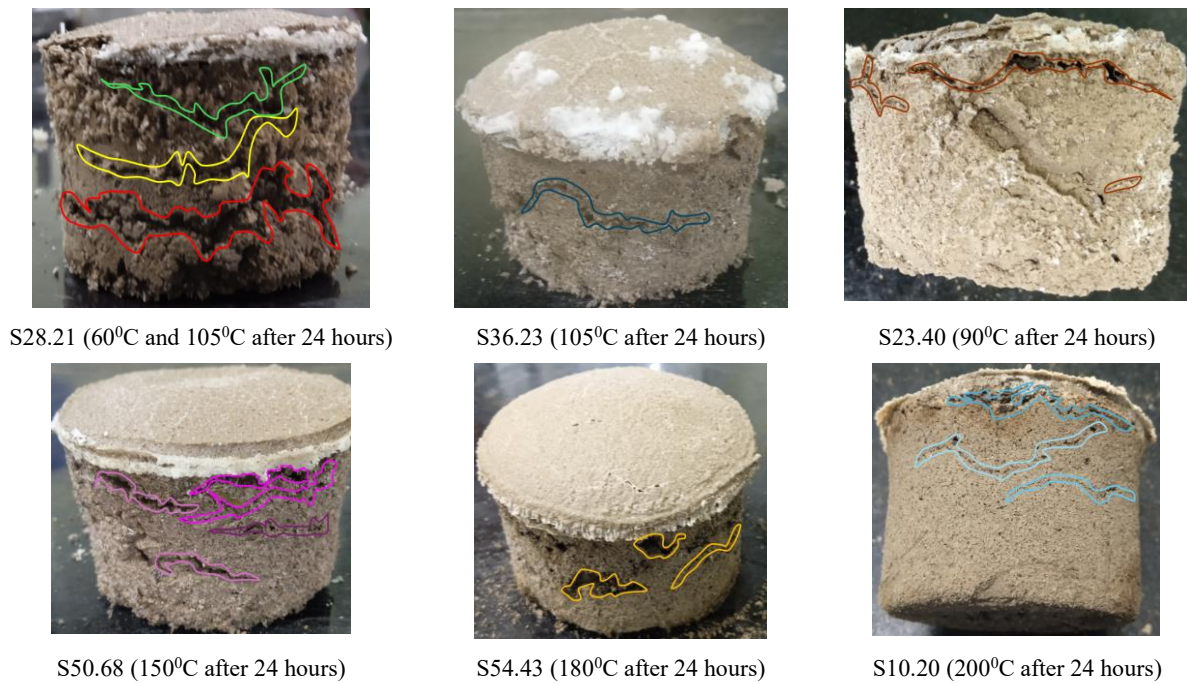


Fig. 2. Crack shapes on the sample body

However, the swell and compaction test of the clay (black cotton soil) was determined particularly when soil mixed with fly ash, polypropylene, and water content was from 10%, 20%; 30%, and 40%. The results describe the crack changes according to the decreasing water content (Miller et al., 2004). An experimental method with the microbial calcite precipitation (MICP) was used by the sprayed deionized water (W), bacteria action (B), and cement concentration (BC). The results show that the camera and microscope support for the crack width changes from 0mm to 2.2mm (Liu et al., 2020). In addition, a compaction Test (ASTMD-2487, 2017) was done with water content from 12.5%, 16.5%, and 20.5% at temperatures $30 \pm 2^{\circ}\text{C}$ and $45 \pm 5\%$. The results of the crack's surface are smaller than the length when the loading value is 1700 kg/m^3 (Tian et al., 2022). Moreover, the crack's length accounts for equation $f(l) = \Delta n / (n \cdot \Delta l)$, where n is the total number of crack segments, and Δn is the number of crack segments whose length ranges between Δl (Tang et al., 2008). However, results show that the length of cracks is determined with the formula:

$$L_{cr} = \lambda_l (n_{orth} + \sqrt{2n_{diag}})$$

whereas, L_{cr} crack length, n_{orth} and n_{diag} respectively represent the numbers of orthogonal and diagonal links between neighboring skeletal pixels, λ_l is the conversion scaling that transforms pixel length to actual length (Wang et al., (2017).

Relationships between cracks, sodium chloride, moisture, and temperature changes from 20°C to 200°C of the samples from S1 to S8 are shown in Fig. 3.

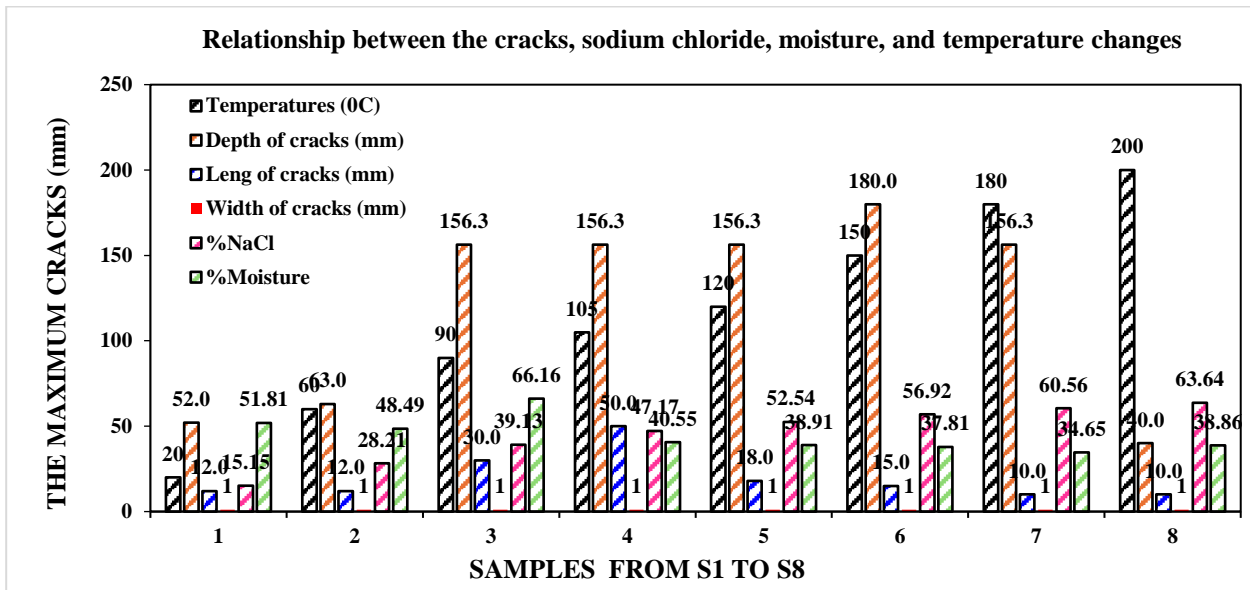


Fig. 3. Relationship between cracks, sodium chloride, moisture, and temperature changes from 20°C to 200°C of the samples from S1 to S8.

On the other hand, the results of the cracks are big and longer with the higher temperature, and the lower cracks with the lower temperature (Rashmisikha and Das, 2022). Moreover, the electrical resistivity method has been used to measure the sample’s cracks at the initial water content of 50.5%. Results of the cracks are not opened fully up yet time $t = 87.0h$ (Tang et al., (2018)). The ratio of the straw is mixed with the soil from 0.5 cm/cm^3 and 1.0 cm/cm^3 . The water content of 43% clay ($\leq 0.002 \text{ mm}$), 32% silt ($0.002 \text{ mm} - 0.02 \text{ mm}$), and 25% sand ($\geq 0.02 \text{ mm}$) at the depth of 0–20 cm, the results of the crack’s width decreased as the straw’s density increased (Wang et al., 2018).

4.3 Relationship between stress and strain

The Unconfined Compression Test (UCT) measured the relationship between the stress and strain at the different loads and temperatures. In the first stage, the stress increase when increasing the strain is clear at 20°C, 60°C, 90°C, and 105°C temperatures, which is shown in Figs 4 to 7.

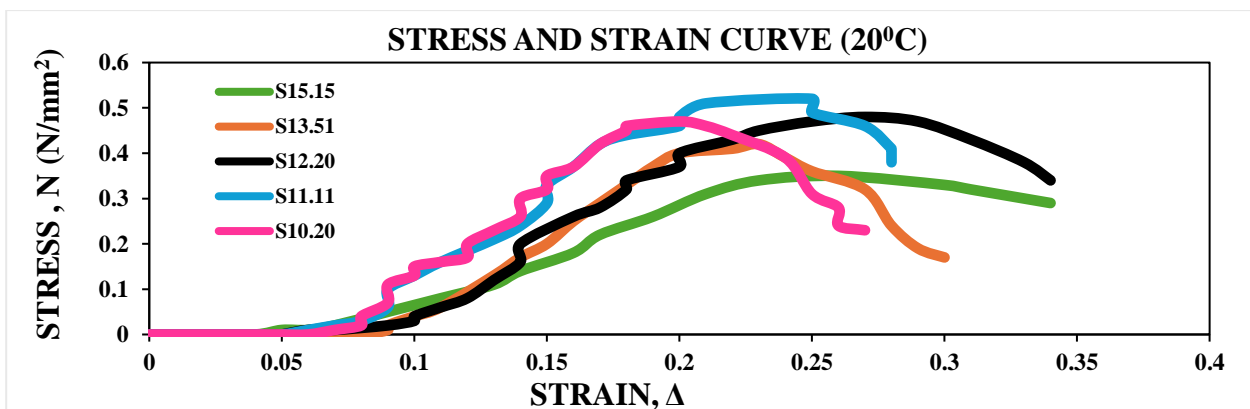


Fig. 4. Relationship between stress and strain (20°C)

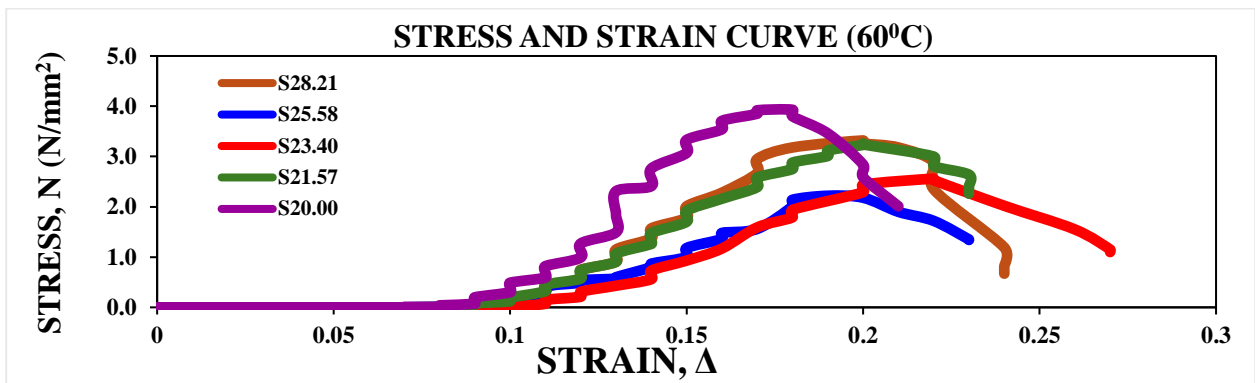


Fig. 5. Relationship between stress and strain (60°C)

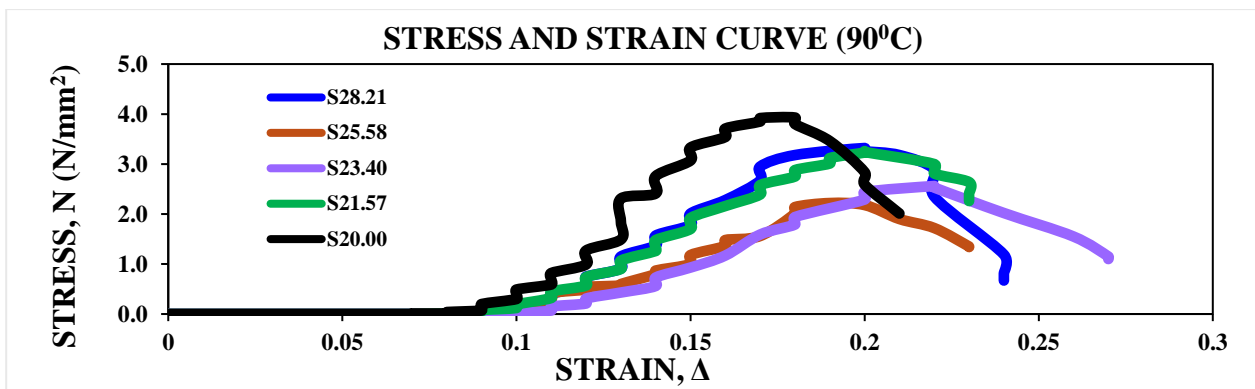


Fig. 6. Relationship between stress and strain (90°C)

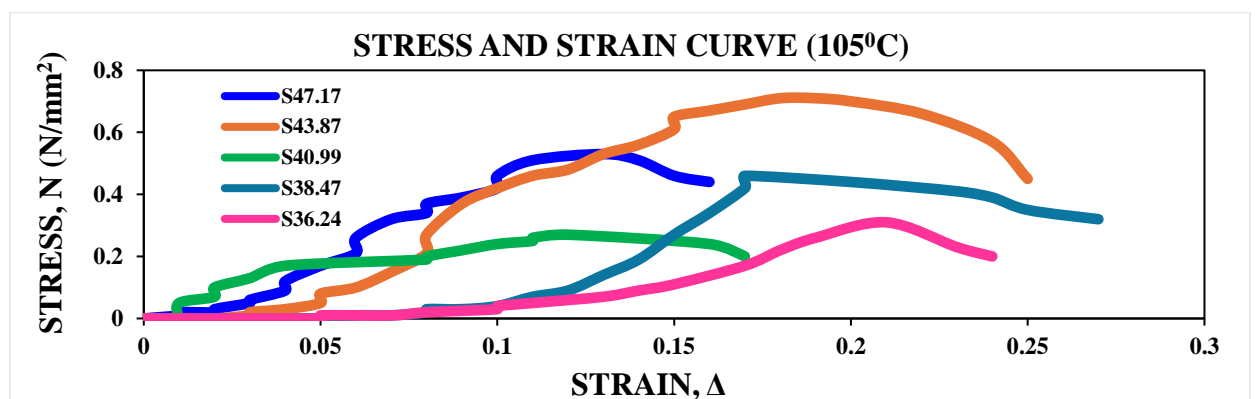


Fig. 7. Relationship between stress and strain (105°C)

In the second stage, the temperature and sodium chloride 'NaCl' concentration increases gradually from 120°C, 150°C, 180°C to 200°C (Figs 8 to 11). The results show that the maximum stress reached 1.403 N/mm² at 180°C temperature; whereas the maximum strain reached 0.51 millimeters at 150°C temperature. However, the results in the crack extensions of the lowest values of displacement and strain of the clay soil (Namdar, 2022).

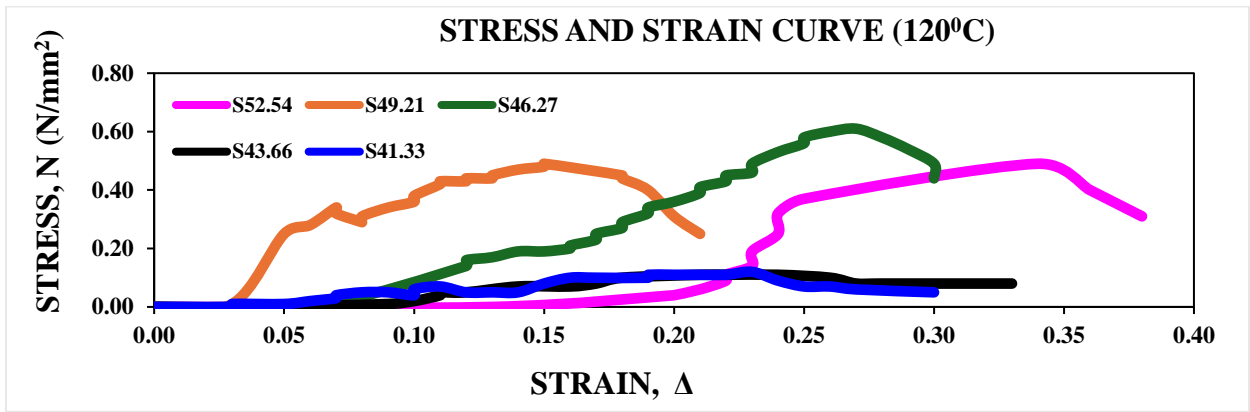


Fig. 8. Relationship between stress and strain (120°C)

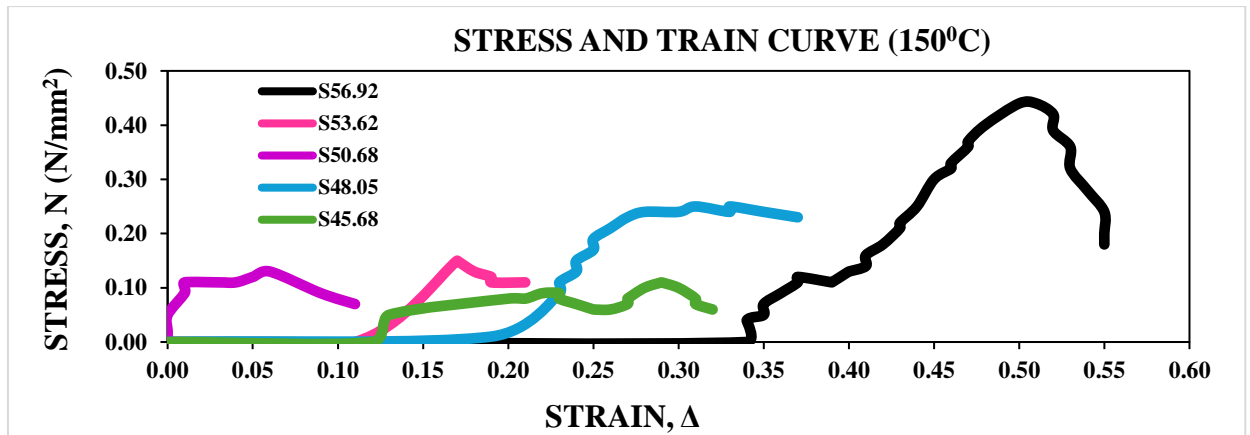


Fig. 9. Relationship between stress and strain (150°C)

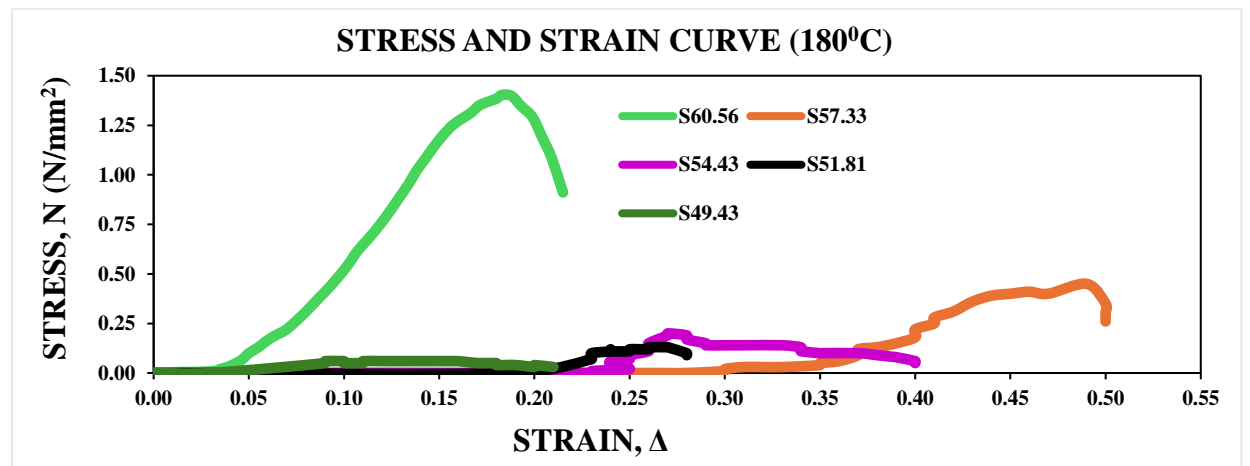


Fig. 10. Relationship between stress and strain (180°C)

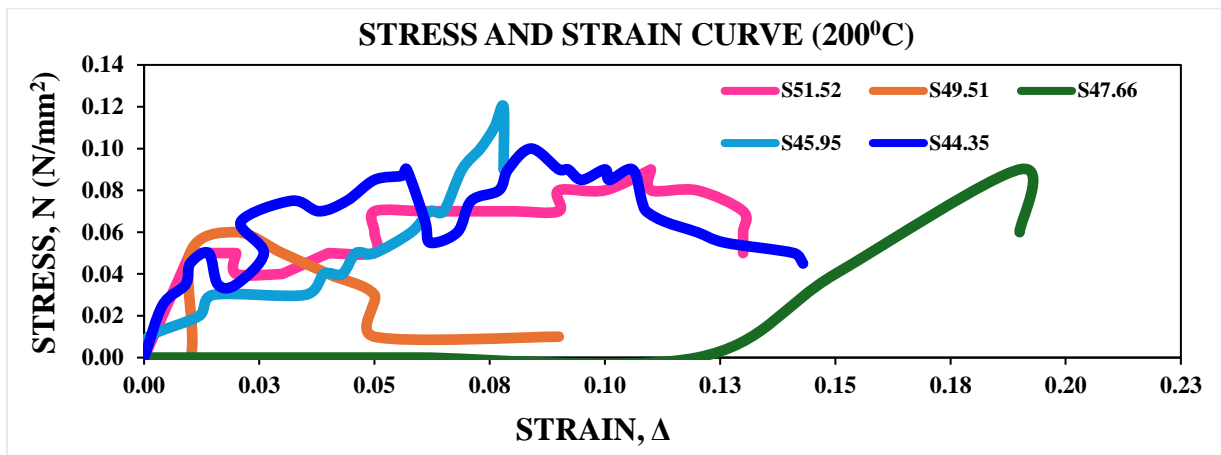


Fig. 11. Relationship between stress and strain (200°C)

4.4 Results of the relationship between loading and displacement at the different temperature variations

The mechanism of load and displacement is inseparable and has a continuous relationship. When the load increases, the displacement of the sample will also increase. The result has caused cracks on the surface of the sample body and the sample has been destroyed. Sample S15.15 corresponding to NaCl content of 15.15% at a temperature of 20°C has a maximum displacement of 7.74 (mm) corresponding to a maximum load of 686.7 (N), which is shown in Fig. 12; other values included S13.51; S12.20; S11.11; S10.20 with the maximum displacement 6.81(mm); 8.15 (mm); 7.35 (mm); 6.01 (mm); maximum loads of 824.04 (N); 941.76 (N); 1020.24 (N); 922.14 (N). Moreover, sample S28.21 with NaCl content of 28.21% at a temperature of 60°C has a maximum displacement of 5.94 (mm) with a maximum load of 6523.65 (N), which is shown in Fig. 13; other values account for S25.58; S23.40; S24.57; S20.00 with the maximum displacement 6.05(mm); 6.51 (mm); 6.04 (mm); 5.28 (mm); maximum loads of 4286.97 (N); 5032.53 (N); 6405.93 (N); 7720.47 (N). However, the big lateral displacement at 4.90m depth is 45 cm (Chu and Yan, 2005). The soft clay and the average area ratio of lateral movement to vertical loading were in the range of 1-2% (Moh and Lin, 2005). However, the lateral displacement of 10m depth at the center of the site for 200 days is 200 mm (Qian et al., 1992). The maximum value of displacement toward the external surcharge obtained 170mm at 8m depth under the surface ground (Song and Kim,2004). On the other hand, sample S39.13 corresponding to NaCl content of 39.13% at a temperature of 90°C has a maximum displacement of 8.92 (mm) with a maximum load of 1294.92 (N); other values show S36.00; S33.33; S31.03; S29.03 with the maximum displacement 4.1(mm); 6.48 (mm); 4.95 (mm); 6.14 (mm); loads of 1608.84 (N); 1373.4 (N); 490.5 (N); 902.52 (N).

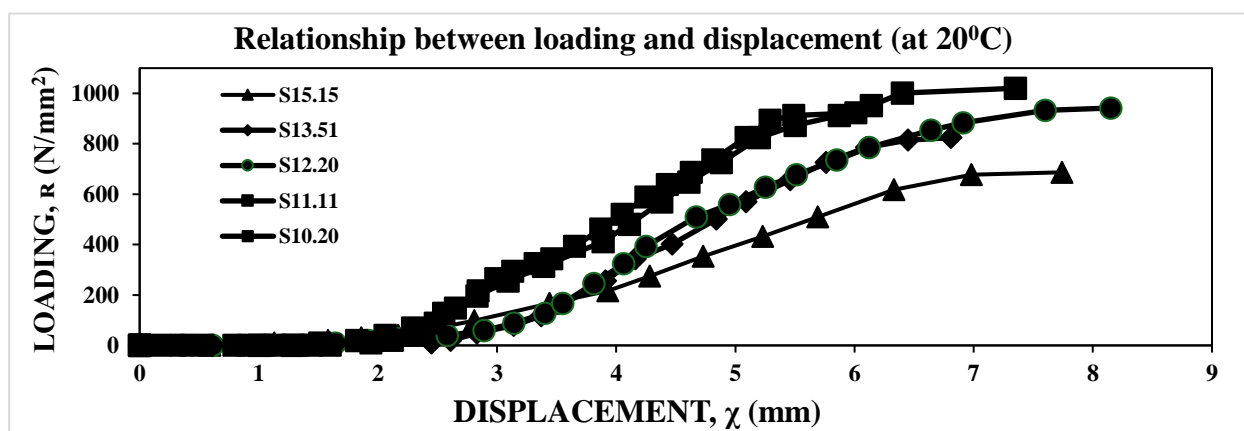


Fig. 12. Relationship between loading and displacement at 20°C

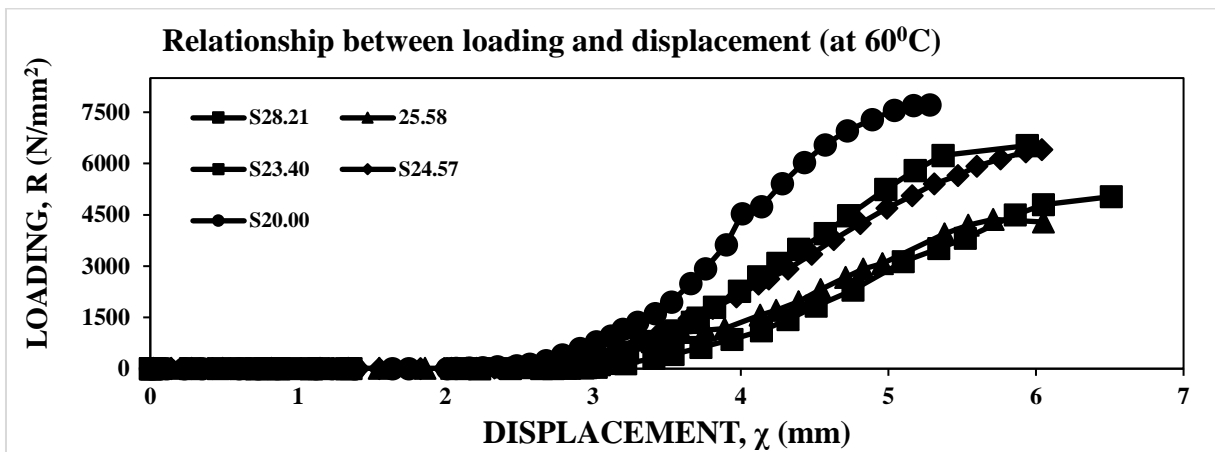


Fig. 13. Relationship between the loading and displacement (at 60°C)

Finite element modeling was used to measure the displacement of the weathering crust from 0m to 2m. The results showed that the horizontal displacement from the center towards the toe is big (Indraratna et al., 2005). Furthermore, Sample S47.17 corresponding to NaCl content of 47.17% at a temperature of 105°C has a maximum displacement of 3.83 mm with a maximum load of 1049.67 (N); other values show S43.86; S40.98; S38.46; S36.23 with the maximum displacement 5.59(mm); 3.73 (mm); 5.17 (mm); 6.22 (mm); with maximum loads of 1402.83 (N); 539.55 (N); 902.52 (N); 608.22 (N).

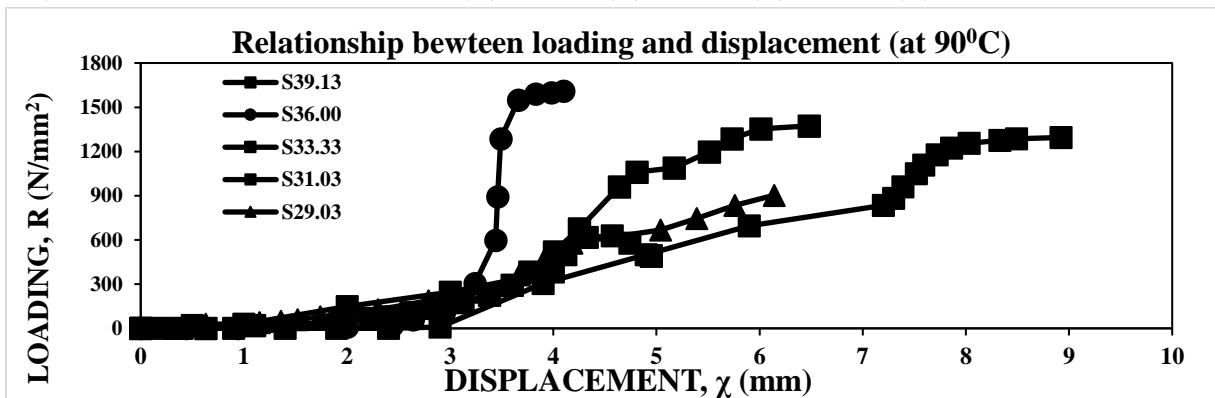


Fig.14. Relationship between the loading and displacement (at 90°C)

However, a preloading clayey deposit by vacuum pressure method with a cap-drain shew the inward lateral displacement obtained 0.5m at 26m depth (Chai et al., 2007). In addition, Sample S52.54 corresponding to NaCl content of 52.54% at a temperature of 120°C has a maximum displacement of 10.14 (mm) corresponding to a maximum load of 971.19 (N); other values show S49.21; S46.27; S43.66; S41.33 with the maximum displacement 4.62 (mm); 8.06 (mm); 7.17 (mm); 6.9 (mm); with maximum loads of 961.38 (N); 1206.63 (N); 225.63 (N); 235.44 (N). However, a modal of the vacuum-drain consolidation was used to measure the pressure distribution and ground lateral displacement. Results show the lateral displacement $\delta_x = 0.25m$ at -17.5 m depth (Chai et al., 2010);The soft ground was measured by a combination loading method without an airtight. Results demonstrate that the maximum inward lateral displacement is 500 mm (Long et al. 2015). The vertical displacement of the sub-layer 2 (4.70-6.15 m) with time in the central part of the Embankments reaches 7% and 4.8% (Marques and Leroueil, 2005). Results presented that there is no horizontal displacement and vertical displacement is small (Saowapakpiboon et al., 2010). In contrast, sample S56.92 corresponding to NaCl content of 56.92% at a temperature of 150°C has a maximum displacement of 14.86 (mm) corresponding to a maximum load of 863.28 (N); other values present S53.62; S50.68; S48.05; S45.68 with the maximum displacement 5.0 (mm); 1.91 (mm); 9.81 (mm); 8.7 (mm); corresponding to maximum loads of 304.11 (N); 255.06 (N); 480.69 (N); 255.63 (N). However, the simulation results show that the vertical displacement is close to the reality measurement data (Shibata et al., 2014). On the contrary, sample S60.56 corresponding to NaCl content of 60.56% at a temperature of 180°C has a maximum displacement of 5.63 (mm) corresponding to a maximum load of 2746.8 (N); other values present S57.33; S54.43; S51.81; S49.43 with the maximum displacement 14.74 (mm); 8.11 (mm); 8.22 (mm); 6.37 (mm); corresponding to maximum loads of 892.71 (N); 372.78 (N); 255.06 (N); 68.67 (N).

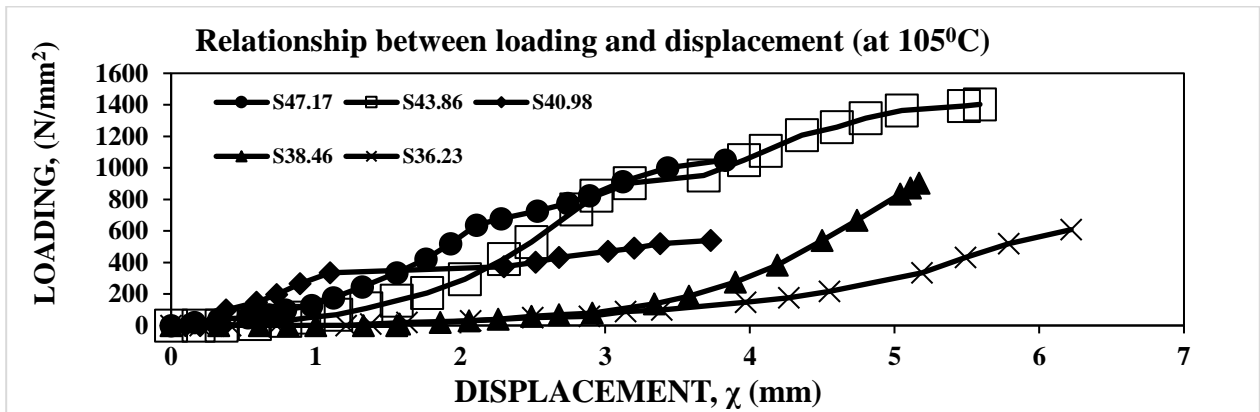


Fig.15. Relationship between loading and displacement (at 105°C)

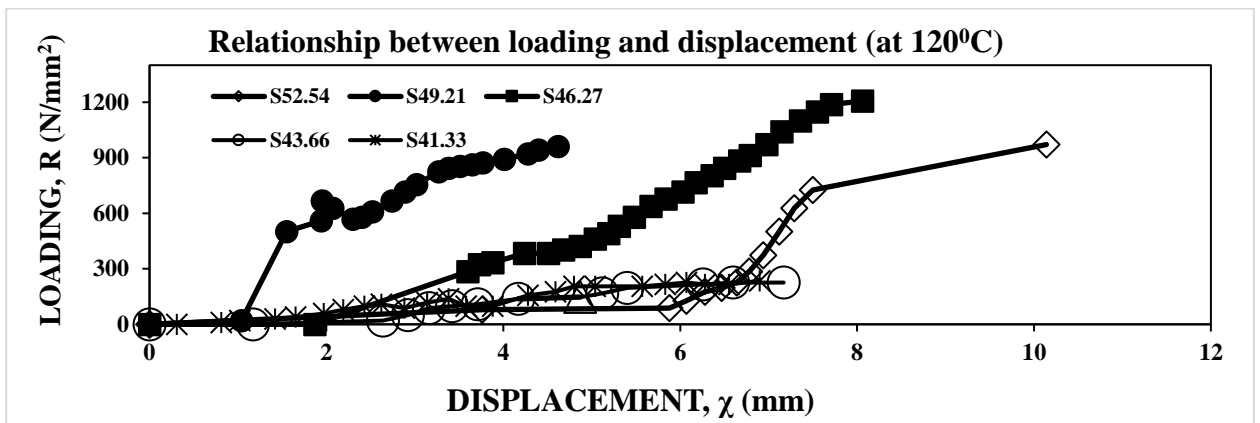


Fig. 16. Relationship between loading and displacement (at 120°C)

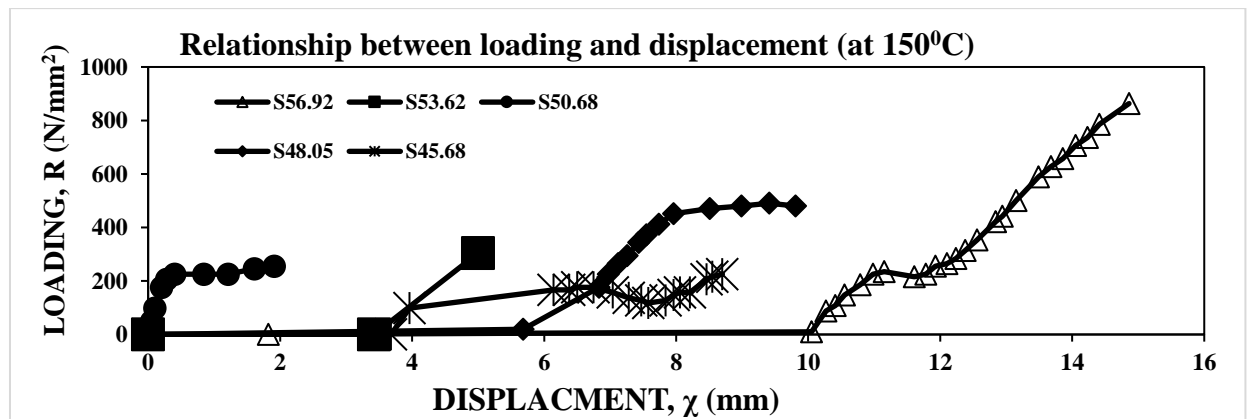


Fig. 17. Relationship between loading and displacement (at 150°C)

However, observation of the soft clay foundation displacements described the lateral displacement decreased with the loading increase by the vertical draining systems (Indraratna et al., 2015). An air-water separation system with a high pressure for vacuum consolidation was used to investigate the maximum lateral displacement. Results presented that the depth value was about 10m where the tip of the sheet piles was located (Teerachaikulpanich and Kosaka, 2015).

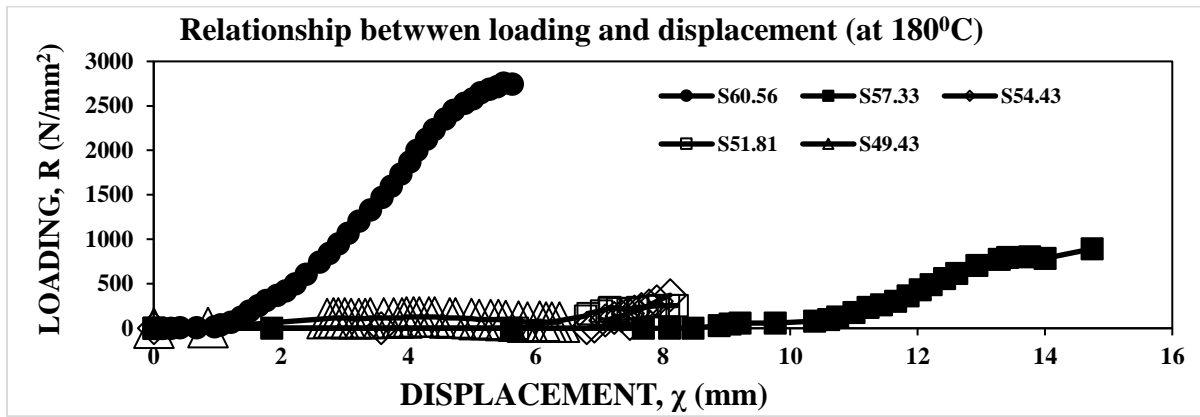


Fig. 18. Relationship between loading and displacement (at 180°C)

Finally, sample S51.52 corresponding to NaCl content of 51.52% at a temperature of 200°C has a maximum displacement of 3.22 (mm) corresponding to a maximum load of 176.58 (N); other values present S49.51; S47.66; S45.95; S44.35 with the maximum displacement 0.61 (mm); 7.54 (mm); 2.34 (mm); 2.51 (mm); corresponding to maximum loads of 117.72 (N); 284.49 (N); 235.44 (N); 196.2 (N). However, results presented no horizontal displacement at 45m depth (Nguyen et al., 2015). Soft ground improvement by pneumatic fracturing method was done to survey the lateral displacement. Results show a slightly smaller displacement than the faster compression loading (Songyu et al., 2016).

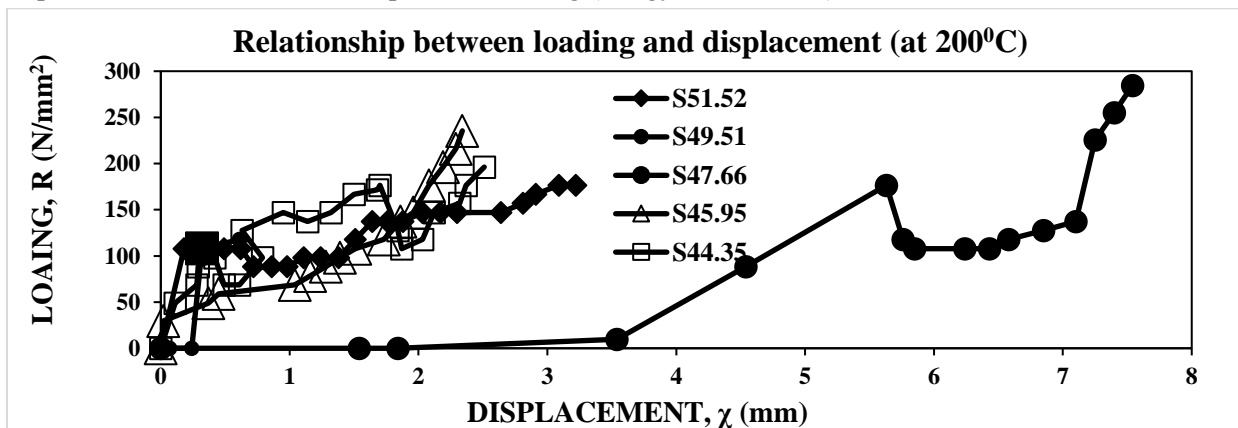


Fig. 19. Relationship between loading and displacement (at 200°C)

4.5 Results of the relationship between the maximum loading and the maximum resistance at sodium chloride ‘NaCl’ variations

The mechanism of load and maximum resistance is an inseparable and shows continuous relationship. When the load is small, sample S11.11 corresponding to NaCl content of 11.11% at a temperature of 20°C has a load resistance of 0.52 (N/mm²) corresponding to a maximum load of 1020.24 (N); other values have a resistance of 3.93 (N/mm²); 0.82 (N/mm²); 0.71 (N/mm²); 0.61 (N/mm²); 0.44 (N/mm²); 1.403 (N/mm²); 0.14 (N/mm²); corresponding to maximum loads of 7720.47 (N); 1608.84 (N); 1402.83 (N); 1206.63 (N); 863.28 (N); 2746.8 (N); 284.49 (N) at temperatures of 60°C; 90°C; 105°C; 120°C; 150°C; 180°C; and 200°C. However, (Thy, 2024a) presents the results show the maximum shear resistance $\tau_{max} = 150.7 \text{ kN/m}^2$ at depth 4.3 m; $\tau_{max} = 159.7 \text{ kN/m}^2$ at depth 7.0 m; $\tau_{max} = 192.6 \text{ kG/cm}^2$ at depth 18.0 m; $\tau_{max} = 219.4 \text{ kN/m}^2$ at depth 27.0 m; $\tau_{max} = 229.2 \text{ kN/m}^2$ at depth 30.3 m; $\tau_{max} = 257.9 \text{ kN/m}^2$ at depth 39.6 m. Moreover, the other research describes the relationship between shear resistance (τ) and depths (D). Results present the shear resistance change in the smallest values by water content containing much more than in the pore holes (Thy, 2024). Finite element method (Plaxis 3D software) and Unconfined Compression Test were used to evaluate the vertical displacement of the soft ground with marine clay ground behaviors under rigid displacement foundation. Results described clearly the vertical displacement of the ground obtains the maximum value = 0.1133 m at 30m depth (Thy, 2024, 2022).

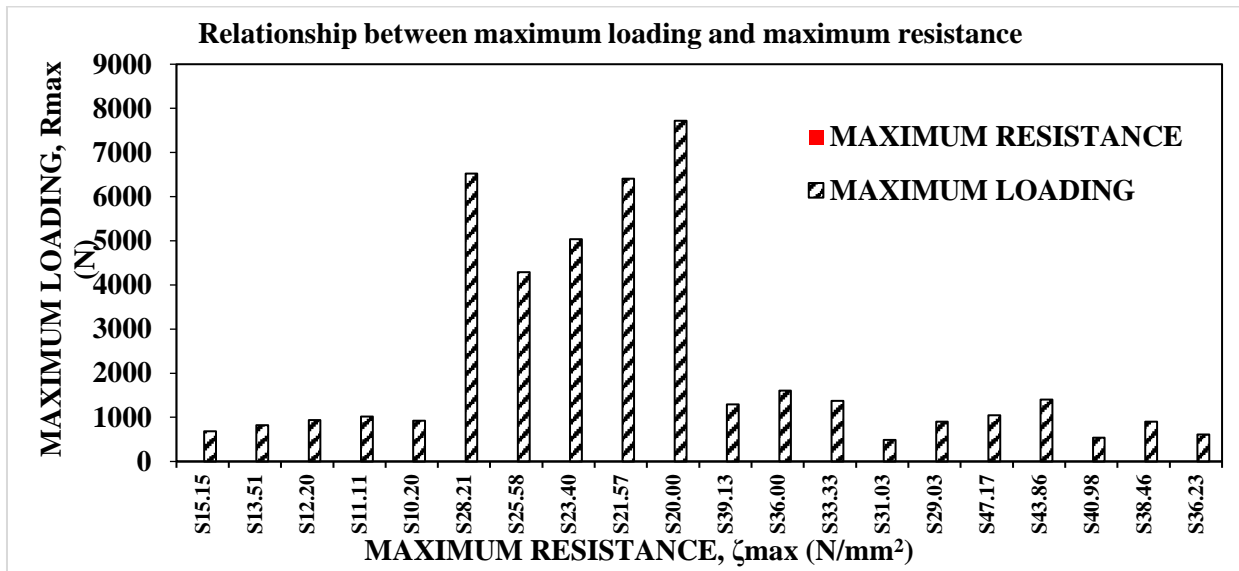


Fig. 20. The maximum load is compared with the lower loading and the lower of Clay’s resistance (at 20⁰C, 60⁰C, 90⁰C, and 105⁰C)

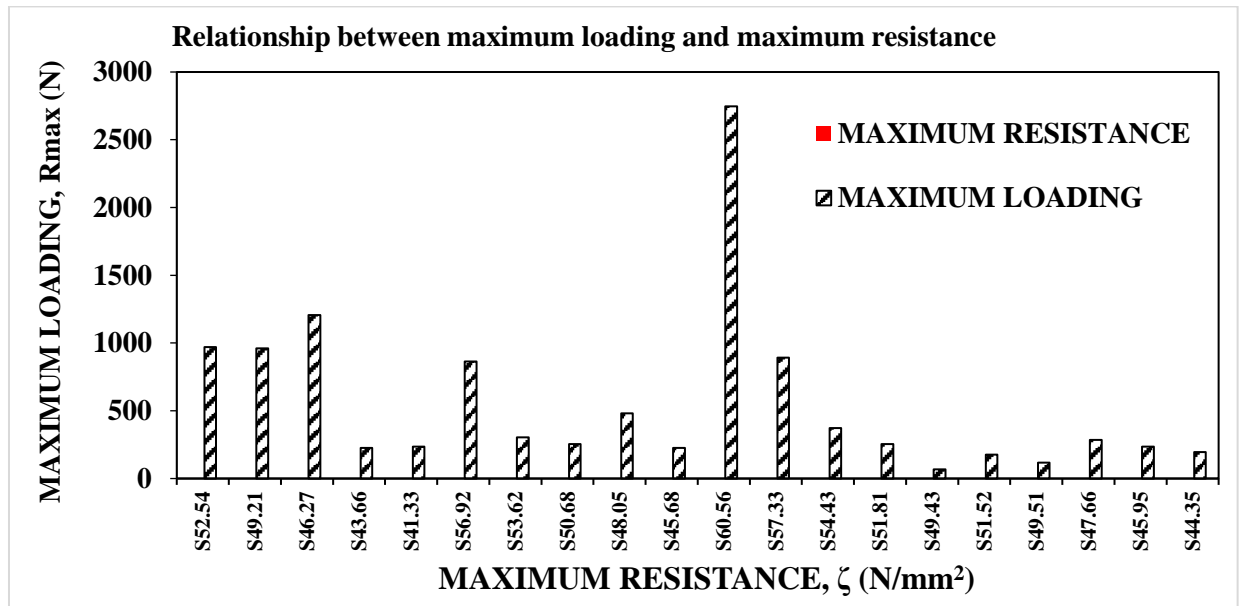


Fig. 21. The maximum load is compared with the lower loading and the lower of Clay’s resistance (at 120⁰C, 150⁰C, 180⁰C, and 200⁰C)

5. Discussion

Cracks evaluation on the specimen body of clay has been evaluated particularly with water content, salt content, temperature, and compressive load variations. Load increases, the displacement, stress, and resistance will change significantly. However, the displacement increased significantly as the distance from the measured point to the test platform decreased (Acosta et al., 2016). The Z-shape of the natural soil with vacuum loading and drain system was done in particular. Results presented the big displacement and deformation as the loading increased (Cai et al., 2017). The Queensland experience is based on the vacuum pressure with the marine clay. The results of the lateral displacement shows from 0.6m to 1.6m and 2.5m depth (Indraratna et al., 2018). On the other hand, the results show the maximum horizontal displacement after one year is 126 mm at a depth of 3.2 m below the ground surface (Indraratna et al., 2016). Experimental evaluation of marine clay slurry was measured by electro-osmosis-vacuum preloading method. The heating affection on the soft deposit behavior was done which effects remarkably the vertical displacement (Wang et al., 2016). The maximum displacement appeared along the slip plane at 8m depth. Results show the potential slip plane through fully of the soil surface and this displacement is a little small (Zhang et al.,

2017). In a case study in coastal China, research on the displacement of the soil ground was done to evaluate the maximum lateral displacement at the ground surface, which obtained 160mm after 150 days (Zhu et al., 2018). An experimental test in the laboratory with the clay-mixed kaolinite using electro-kinetic geosynthetics and electro-osmotic consolidation combined with vacuum preloading. Results showed that the maximum lateral displacement reached 33mm (Zhang L and Hu, 2018). The dredged fill was done to control the displacement. The influence of the clogging of the dredged to the lateral displacement and uneven reinforcement forms a dense zone (Xu et al., 2020).

6. Conclusion

Research on the defects (cracks) of clay mixing Sodium Chloride 'NaCl' was done to measure the stress, strain, resistance, and displacement with loading variations. Temperatures were used from 20°C to 200°C. Sodium Chloride 'NaCl' concentration varied from 10.20% to 60.56%. The research results describe clear defects (cracks) where they appear much more on the body sample. The sodium chloride 'NaCl' concentration has many results in preventing the crack from appearing. Moreover, the increasing the loading and the temperature, the displacement, stress, strains, and resistances increased respectively. Finally, these research results are useful to refer to such surveys, design, and construction in geology and civil engineering whereas marine original clay soils are often affected by salt concentration.

Acknowledgments

Authors thank the anonymous reviewers for improving the paper.

Literature - References

1. Acosta L N P, Santiago EA L, Núñez P V M, Ossa A, Mendoza M J, Shelley O E, Botero E, 2019, Performance of a test embankment on very soft clayey soil improved with rain-to-drain vacuum preloading-technology, Geotextiles and Geo-membranes, 47, 1-14. <https://doi.org/10.1016/j.geotextmem.2019.103459>.
2. Alizadeh Akram and Dargahi Khatoon (2024), Mechanism of Ivughli salt dome exhumation, northwestern Iran, Geology, Ecology, and Landscapes. <https://doi.org/10.1080/24749508.2024.2373494>.
3. Bo-wei Zhang, Ze-qun Zhang, Qi-juan Dong, Jun-sheng Wu, Ning Zhuang, Peng-cheng Zuo, Xiao-gang Li, 2024, Electrochemical corrosion behavior of nanostructured BCC-Al_{0.5}CoCrFeNi_{0.4} high-entropy alloy in sodium chloride solution, Trans. Nonferrous Met. Soc. China 34, 1908-1921. [http://10.1016/S1003-6326\(24\)66515-5](http://10.1016/S1003-6326(24)66515-5).
4. Chai J, Miura N, Bergado D T, 2007, Preloading clayey deposit by vacuum pressure with cap - drain: Analyses versus performance, Geotextiles and Geo-membranes, 26, 1001-1004. <https://doi.org/10.1016/j.geotextmem.2007.10.004>
5. Chai J, Hong Z, Shen S, 2010, Vacuum- drain consolidation induced pressure distribution and ground deformation, Geotextiles and Geo-membranes, 28, 525-535. <https://doi.org/10.1016/j.geotextmem.2010.01.003>.
6. Cai Y, Qiao H, Wang J, Geng X, Wang P, Cai Y, 2017, Experimental tests on effect of deformed prefabricated vertical drains in dredged soil on consolidation via vacuum preloading, Engineering Geology, 222, 10-19. <https://doi.org/10.1016/j.enggeo.2017.03.020>.
7. Colpo Angélica,
Sabrina Vantadori, Leandro Friedrich, Andrea Zanichelli, Camilla Ronchei, Daniela Scorza, Ignacio Iturrioz, 2022, Crack path estimation in the shot-earth 772 by a discrete element method, Procedia Structural Integrity 41 260–265, <https://doi.org/10.1016/j.prostr.2022.05.030>.
8. Chu J, Yan S W, 2005, Application of the Vacuum Preloading Method in Soil Improvement Projects, Elsevier Geo-engineering book series, chapter 3, volume 3, 91-117. [https://doi.org/10.1016/S1571-9960\(05\)80006-0](https://doi.org/10.1016/S1571-9960(05)80006-0).
9. Greve A, M.S. Andersen, R.I. Acworth, 2010. Investigations of soil cracking and preferential flow in a weighing lysimeter filled with cracking clay soil, Journal of Hydrology, 393, 105–113, <https://doi.org/10.1016/j.jhydrol.2010.03.007>
10. Chuanxin Hou, Fushan Li, Hideo Kimura, Qiuyu Li, Liyuan Liu, Qiqi Chu, Jinmiao Wu, Guohua Fan, Wei Du, 2023, Sodium chloride assisted synthesis of porous magnetic carbon nanocomposites containing cobalt nanoparticles for high-performance electromagnetic wave-absorption, journal of materials research and technology, 2 5, 5148 e 5158. <https://doi.org/10.1016/j.jmrt.2023.07.010>.
11. Indraratna B, Kan E M, Potts D, Rujikiatkamjorn C, Sloan W S, 2016, Analytical solution and numerical simulation of vacuum consolidation by vertical drains beneath circular embankments, Computers and Geo-technics, 80, 83-96. <https://doi.org/10.1016/j.compgeo.2016.06.008>.

12. Indraratna B, Rujikiatkamjorn C, Balasubramaniam A S, Wijeyakulasuriya V, 2005, Predictions and Observations of Soft Clay Foundations Stabilized with Geo-Synthetic Drains and Vacuum Surcharge, Elsevier Geo-Engineering book series, chapter 7, volume 3, 199-229. [https://doi.org/10.1016/S1571-9960\(05\)80010-2](https://doi.org/10.1016/S1571-9960(05)80010-2).
13. Indraratna B, Rujikiatkamjorn C, Balasubramaniam A S, Wijeyakulasuriya V, 2015, Predictions and Observations of Soft Clay Foundations Stabilized with Geo-Synthetic Drains and Vacuum Surcharge, 4th Edition, Canada. [https://doi.org/10.1016/S1571-9960\(05\)80010-2](https://doi.org/10.1016/S1571-9960(05)80010-2).
14. Indraratna B, Rujikiatkamjorn C, Baral P, Ameratunga J, 2018, Performance of marine clay stabilized with vacuum pressure: Based on Queensland experience, Journal of Rock Mechanics and Geotechnical Engineering, 2, 1-14. <https://doi.org/10.1016/j.jrmge.2018.11.002>.
15. Long P V, Nguyen L V, Bergado D T, Balasubramaniam A S, 2015, Performance of PVD improved soft ground using vacuum consolidation methods with and without airtight membrane, Geotextiles and Geo-membranes, 47, 1-11. <https://doi.org/10.1016/j.geotexmem.2015.05.007>.
16. Bo Liu, Cheng Zhu, Chao-Sheng Tang, Yue-Han Xie, Li-Yang Yin, Qing Cheng, Bin Shi, 2020. Bio-remediation of desiccation cracking in clayey soils through microbial induced calcite precipitation (MICP), Engineering Geology, 264, 105-389, <https://doi.org/10.1016/j.enggeo.2019.105389>.
17. Moh C Z, Lin P, 2005, Case Study of Ground Improvement Work at the Suvarnabhumi Airport of Thailand, Elsevier Geo-Engineering book series, chapter 3, volume 3, 159-198. <https://doi.org/10.1016/B978-0-08-100192-9.00006-5>.
18. Marques M E S, Leroueil S, 2005, Pre-consolidating Clay Deposit by Vacuum and Heating in Cold Environment, Elsevier Geo-Engineering book series, chapter 36, volume 3, 1045-1063. [https://doi.org/10.1016/S1571-9960\(05\)80039-4](https://doi.org/10.1016/S1571-9960(05)80039-4).
19. Carol J. Miller, P.E., M.ASCE, and Sami Rifai, P.E, 2004, Fiber Reinforcement for Waste Containment Soil Liners, J. Environ. Eng, 130 (8): 891-895, <https://doi.org/10.1061/~ASCE0733-9372~2004-130:8~891>.
20. Nguyen S H, Tashiro M, Inagaki M, Yamada S, Noda T, 2015, Simulation and evaluation of improvement effects by vertical drains/vacuum consolidation on peat ground under embankment loading based on a macro-element method with water absorption and discharge functions, Soils and Foundations, 55(5), 1044-1057. <https://doi.org/10.1016/j.sandf.2015.09.007>.
21. Ni P, Xu K, Mei G, Zhao Y, 2018, Effect of vacuum removal on consolidation settlement under a combined vacuum and surcharge preloading, Geotextiles and Geo-membranes, 47, 12-22. <https://doi.org/10.1016/j.geotexmem.2018.09.004>.
22. Neyamadpour A, 2018, Detection of subsurface cracking depth using electrical resistivity tomography: A case study in Masjed - Soleiman, Iran, Construction and Building Materials 191, 1103-1108, <https://doi.org/10.1016/j.conbuildmat.2018.10.027>.
23. Namdar A, 2022, Impact of soil crack on embankment seismic resistance, Procedia Structural Integrity, 39 47-56, <https://doi.org/10.1016/j.prostr.2022.03.071>.
24. Qian H, Zhao W B, Cheung Y K, Lee P K K, 1992, The theory and practice of vacuum preloading, Computers and Geo-technics, 13(2), 103-118. [https://doi.org/10.1016/0266-352X\(92\)90027-Q](https://doi.org/10.1016/0266-352X(92)90027-Q).
25. Rashmisikha B and M.R.das, 2022, An experimental study on evaluation of fiber Reinforced-Fly ash stabilized black cotton soil as a sustainable subgrade material, Materials Today: Proceedings 62, 6182-6188, <https://doi.org/10.1016/j.matpr.2022.05.044>.
26. Songyu L, Dingwen Z, Guangyin D, Wenjun H, 2016, A New Combined Vacuum Preloading with Pneumatic Fracturing Method for Soft Ground Improvement, In proceeding of 3th International Conference on Transportation Geo-Technics (ICTG 2016), Nanjing, China. <https://doi.org/10.1016/j.proeng.2016.06.057>.
27. Song S Y, Kim T H, 2004, Improvement of estuarine marine clays for coastal reclamation using vacuum - applied consolidation method, In proceeding of 31th Ocean Engineering, South Korea, 1999-2010. <https://doi.org/10.1016/J.OCEANENG.2004.05.004>.
28. Saowapakpiboon J, Bergado D T, Voottipruex P, Lam L G, Nakakuma K, 2010, PVD improvement combined with surcharge and vacuum preloading including simulations, Geotextiles and Geo-membranes, 29, 74-82. <https://doi.org/10.1016/j.geotexmem.2010.06.008>.
29. Shibata T, Murakami A, Fujii M, 2014, Prediction of embankment behavior of regulating reservoir with foundation improved by vacuum consolidation method, Soils and Foundations, 54(5), 938-954. <https://doi.org/10.1016/j.sandf.2014.09.008>.

30. Chaosheng Tang, Bin Shi, Chun Liu, Lizheng Zhao, Baojun Wang, 2008. Influencing factors of the geometrical structure of surface shrinkage cracks in clayey soils, *Engineering Geology*, 101, 204–217, <http://doi:10.1016/j.enggeo.2008.05.005>.
31. Chao-Sheng Tang, De-Yin Wang, Cheng Zhu, Qi-You Zhou, Shi-Kang Xu, Bin Shi, 2018, Characterizing drying-induced clayey soil desiccation cracking process using electrical resistivity method, *Applied Clay Science*, 152 (2018), 101–112, <https://doi.org/10.1016/j.clay.2017.11.001>.
32. Ben-Gang Tian, Qing Cheng, Chao-Sheng Tang, Hao Zeng, Jin-jian Xu, Bin Shi, 2022. Effects of compaction state on desiccation cracking behavior of a clayey soil subjected to wetting-drying cycles, *Engineering Geology*, 302 106-650, <https://doi.org/10.1016/j.enggeo.2022.106650>.
33. Teerachaikulpanich N, Kosaka T, 2015, High Pressure for Vacuum Consolidation Method Using Air-Water Separation System, 3rd Edition, Japan. <https://doi.org/10.1016/B978-0-08-100192-9.00010-7>.
34. Thy T. Doan, 2022. Evaluation of the vertical displacement of the circular foundation on the over-consolidation ground in Phu Quoc Island, Kien Giang province, Viet Nam. Proceedings of the 6th International Conference on Civil Engineering for Sustainable Development (ICCESD 2022), 10~12 February 2022, KUET, Khulna, Bangladesh (ISBN-978-984-35-1972-6). http://103.157.135.50/proc_2022/Papers/GTE-01125.pdf.
35. Thy T. Doan^a, 2024. Experiment measurement of the cracks by the Sodium Chloride concentration and temperature changes, *J. Materialstoday: Proceedings*. <https://doi.org/10.1016/j.matpr.2024.02.024>.
36. Thy T. Doan^b, 2024. Comparison between numerical analysis and experiment for the dry density and shear resistance variations with different depths (groundwater level variations). *J. Geology, Ecology, and Landscapes*. <https://doi.org/10.1080/24749508.2023.2254011>.
37. Wang Ce, Zhan-yu Zhang, Yang Liu, Shi-min Fan, 2017. Geometric and fractal analysis of dynamic cracking patterns subjected to wetting-drying cycles, *Soil & Tillage Research*, 170 1–13, <http://dx.doi.org/10.1016/j.still.2017.02.005>.
38. Wang Ce, Zhan-yu Zhang, Shi-min Fan, Richwell Mwiya, Mei-xiang Xie, 2018. Effects of straw incorporation on desiccation cracking patterns and horizontal flow in cracked clay loam, *Soil & Tillage Research*, 182, 130–143, <https://doi.org/10.1016/j.still.2018.04.006>.
39. Wang J, Ma J, Liu F, Mi W, Cai Y, Fu H, Wang P, 2016, Experimental study on the improvement of marine clay slurry by electro-osmosis-vacuum preloading, *Geotextiles and Geo-membranes*, 44, 615-622. <https://doi.org/10.1016/j.geotexmem.2016.03.004>.
40. Xu H B, He N, Jiang B Y, Zhou Z Y, Zhan J X, 2020, Experimental study on the clogging effect of dredged fill surrounding the PVD under vacuum preloading, *Geotextiles and Geo-membranes*, 188, 121-125. <https://doi.org/10.1016/j.geotexmem.2020.03.007>.
41. Zhang Z, Ye B G, Xu Y, 2017, Comparative analysis on the performance of vertical drain improved clay deposit under vacuum or surcharge loading, *Geotextiles and Geo-membranes*, 46, 146-154. <https://doi.org/10.1016/j.geotexmem.2020.03.007>.
42. Zhang L, Hu L, 2018, Laboratory tests of electro-osmotic consolidation combined with vacuum preloading on kaolinite using electro-kinetic geo-synthetics, *Geotextiles and Geo-membranes*, 47, 166-176. <https://doi.org/10.1016/j.sandf.2018.12.015>.
43. Zhu W, Yan J, Yu G, 2018, Vacuum preloading method for land reclamation using hydraulic filled slurry from the sea: A case study in coastal China, *Ocean Engineering*, 152, 286-299. <https://doi.org/10.1016/j.oceaneng.2018.01.063>.
44. Ulén Barbro, Gunborg Alex, Jenny Kreuger, Annika Svanbäck & Ararso Etana, 2012, Particulate-facilitated leaching of glyphosate and phosphorus from a marine clay soil via tile drains, *Acta Agriculturae Scandinavica, Section B – Soil & Plant Science*, 62:sup2, 241-251. <https://doi.org/10.1080/09064710.2012.697572>.
45. Laptop 3 Mien company, Image J software, 2024. <https://laptop3mien.vn/tai-imagej-2024-link-google-da-test-100-va-huong-dan-cai-dat-full/>